Received: 31 December 2021 | Revised: 30 August 2022 | Accepted: 14 September 2022

DOI: 10.1002/we.2785

RESEARCH ARTICLE

WILEY

A time-varying formulation of the curled wake model within the FAST.Farm framework

Emmanuel Branlard | **Luis A Martínez-Tossas** | **Jason Jonkman**

National Wind Technology Center, National Renewable Energy Laboratory, Golden, Colorado, USA

Correspondence
Emmanuel Branlard, National Wind Technology Center, National Renewable Energy Laboratory, Golden, CO, USA.
Email: emmanuel.branlard@nrel.gov

Funding information
US Department of Energy Office of Energy Efficiency and Renewable Energy Wind Energy Technologies Office

Abstract

In this article, we present a time-varying formulation of the curled wake model that we implemented in FAST.Farm. The curled wake model, originally developed for steady-state conditions, is used to produce realistic wake profiles behind a wind turbine in yawed (or skewed) conditions. We begin by introducing the key elements of the FAST.Farm framework. Then, after briefly summarizing the original wake dynamics formulation of FAST.Farm based on a polar wake profile, we present the new time-varying formulation of the curled wake model, compare the two, and highlight the differences with the original curled wake model. After discussing some implementation details, we present different applications with increasing levels of complexity: single turbine with uniform and turbulent inflow, fixed and transient yaw, and multiple turbines. We verify our results using the original FAST.Farm implementation and large-eddy simulations. The results with the new curled wake model are improved compared to the original implementation, as they include cross-flow velocities and wake asymmetry. Yet, large-eddy simulation results show a more pronounced lateral convection of the wake and a stronger concentration of vorticity at the top vortex. The new curled wake implementation in FAST.Farm should enable the calculation of not only generator power but also wind turbine structural loads for applications involving intentional or unintentional skewed flow and wind-farm control involving wake steering.

KEYWORDS
curled wake, dynamic wake meandering, FAST.Farm, skewed flow, yaw

1 | INTRODUCTION

Capturing the wake aerodynamics behind yawed wind turbines has become increasingly important as wind turbines are densely packed in wind farms and wake-steering control strategies through intentional yaw misalignment are being implemented.[1,2] Earlier development of skewed* rotor aerodynamics focused on the determination of the induced velocities at the rotor plane. The lifting disk model of Glauert[3] and the vortex model of Coleman[4] form the basis of the yaw (or skewed flow) corrections used in most blade element momentum codes. The vortex model of Coleman uses a rigid vortex cylinder representation of the wake. It has been extended in the past[5] to obtain the velocity field at the rotor, near-wake, and

*In this paper, the term "skewed" is used to include both yawed and titled configurations.

induction zone.[6] But the model cannot represent the far wake accurately. Indeed, the wake vorticity surface will not stay rigid; it will change shape due to its self-induced velocity, and it will diffuse downstream. Advanced models have recently been developed to account for time variation of the vorticity surface shape,[7] leading to improved formulations.

Modeling[8–11] and experimental[12–15] campaigns investigating the wake of yawed wind turbines have noted two characteristics: (1) in planes downwind of the rotor and normal to the freestream, two zones of strong and opposite vorticity are observed at the top and bottom of the wake; (2) the wake curls up and forms a "curled wake" (also referred to as "kidney shape"). The first observation is a direct consequence of the tangential vorticity coming in and out of the planes normal to the freestream, because for the most part, the wake vorticity is parallel to the rotor plane. Such aspect is already accounted for in rigid vorticity-based models.[5] The second observation is a consequence of the vorticity transport caused by induced velocities in the cross-flow directions.

Based on these observations, several models have been devised to compute time-averaged wake dynamics in yawed conditions using the collection of vortices shed from the rotor plane.[9–11,16] In this work, we focus on the curled wake model.[11,17] In the curled wake model, a simplified version of the Reynolds-averaged Navier–Stokes equations are solved numerically, and the cross-flow-induced velocities are determined using a distribution of infinite vortex lines. A vortex cylinder approach could similarly be used to obtained the cross-flow velocities.[18]

In this work, we extend the curled wake model by including a time-varying formulation. This new formulation is incorporated into the midfidelity engineering tool FAST.Farm[19] to compute the time-dependent spatially filtered wake of wind farms with turbines that experience skewed flow. FAST.Farm is a midfidelity multiphysics engineering tool for predicting the power performance and structural loads of wind turbines within a wind farm.[20] The use of FAST.Farm facilitates the incorporation of quasi-steady models, such as the curled wake model, into a time-varying formulation, because FAST.Farm uses a mixed Eulerian–Lagrangian formulation. In this formulation, the wake dynamics are computed in a quasi-steady meandering frame of reference and convected downstream in a fashion similar to the dynamic wake meandering model.[21] A better representation of the wake dynamics in skewed-flow conditions is expected to lead to improved estimations of wind turbine loads.[20]

We begin this article by introducing the key elements of the FAST.Farm framework. Then, after briefly summarizing the original wake dynamics formulation of FAST.Farm, we present the new time-varying formulation of the curled wake model and compare the two. We also examine differences between the original model and the new time-varying curled wake model. After discussing some implementation details, we present different applications with increasing levels of complexity, and we verify our results using the original FAST.Farm implementation and large-eddy simulations.

2 | FORMULATIONS

We have implemented an unsteady version of the curled wake model within the FAST.Farm framework. FAST.Farm already accounts for the Lagrangian convection of the flow quantities, which greatly simplifies the implementation. We begin by providing an introduction to the theory behind FAST.Farm. Then, we provide the formulations of the original wake model and the newly implemented unsteady curled wake model. We discuss implementation details in Section 2.4.

2.1 | Principles of FAST.Farm

In this section, we provide a brief overview of FAST.Farm. The reader is referred to the documentation in Jonkman and Shaler[19] for additional details on the theory and usage of FAST.Farm.

2.1.1 | Overview of FAST.Farm modules

FAST.Farm is an open source solver for wind farm simulations developed by the National Renewable Energy Laboratory (NREL). The tool is based on the dynamic wake meandering model[21] but includes advanced corrections. FAST.Farm comprises three main modules: OpenFAST (and its submodules), WakeDynamics, and the Ambient Wind and Array Effects (AWAE) module. The modules are illustrated in Figure 1.

An instance of the OpenFAST and WakeDynamics modules is invoked for each turbine, whereas AWAE is used at the wind farm level. The three modules are wrapped together within the FAST.Farm glue code. We briefly describe the modules below.

- OpenFAST performs the full aero-hydro-servo-elastic simulation of the turbine. OpenFAST receives the inflow from AWAE; the inflow consists of turbulence and wakes from neighboring turbines.
- The WakeDynamics module solves for the wake of a given turbine. To achieve this, the wake is discretized into a finite number of wake deficit planes, which are convected using an inflow velocity provided by AWAE. The flow dynamics (diffusion, expansion) are obtained by solving the

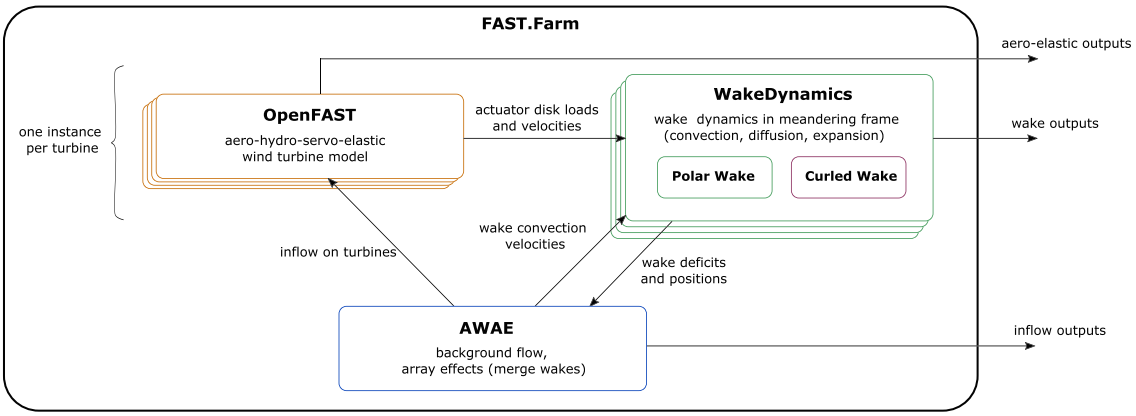

FIGURE 1 Main modules of FAST.Farm, functionalities, and data flow

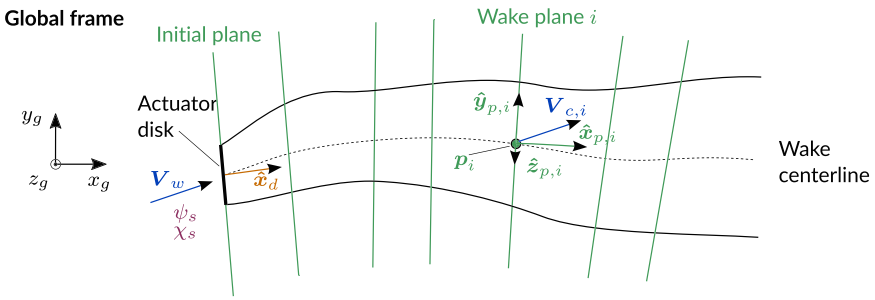

FIGURE 2 Wake planes in the global frame, as used in the module WakeDynamics

thin shear layer approximation of the Navier–Stokes equation in the meandering frame of reference with closure accounted for via an eddy viscosity model. The initial wake deficits are determined using an actuator disk model in which the loads are obtained by the azimuthal averaging of the blade loads computed by the OpenFAST module. We will discuss the WakeDynamics module in more details in the subsequent paragraphs, as it is the main component that is modified to include the curled wake model.

- The AWAE module handles wind and array effects. It loads a turbulent background flow over the entire wind farm, using a higher resolution near the turbines for increased accuracy of the aeroelastic response. AWAE receives the position and wake deficits of each wake plane from each turbine and merges these wake deficits together and with the background flow. From this, AWAE can compute the inflow velocities requested by the two other modules. AWAE provides the local inflow velocities for all the turbines handled by the different instances of OpenFAST. AWAE computes the convection velocity of the wake planes using a characteristic volume surrounding the wake planes.

In the following sections, we focus on the modeling aspects that are different between the original formulation in FAST.Farm and the new curled wake formulation. Most of the differences concern the equations solved in the meandering frame of reference, and therefore in the WakeDynamics module. The implementation changes related to the AWAE module are given in Section 2.4.

2.1.2 | Wake planes, skew angle, and meandering frame of reference

We illustrate the notion of wake planes in Figure 2.

The WakeDynamics module stores a set of planes, each of them containing the wake velocity deficit at the location of the plane. Each wake plane is attributed a local coordinate system ($\hat{\boldsymbol{x}}_{p,i}, \hat{\boldsymbol{y}}_{p,i}, \hat{\boldsymbol{z}}_{p,i}$) and a center position ($\boldsymbol{p}_i$), where i is the plane index, and the overhat symbol indicates unit vectors (without this symbol, the coordinate axis is implied). The planes keep their initial orientation and coordinate system throughout the simulation. During a time step, the velocity deficits carried by each plane evolve according to the fluid dynamics equations given in subsequent sections, and the position of each wake is updated by convecting them with a local velocity, $\boldsymbol{V}_{c,i}$, computed by AWAE in a characteristic volume surrounding the wake plane. At the end of a time step, a new plane (with index $i = 0$) is introduced at the actuator disk position and the existing

planes are re-indexed. To account for the slow variation of the rotor induction, the WakeDynamics module introduces a time filter on most of its inputs,[19] which we will further note using an overbar. We will discuss this time filter in Section 3.5.

The plane coordinate system is defined as follows[†]: The unit vector $\hat{\boldsymbol{x}}_{p,0}$ is set to the time-filtered value of the actuator disk normal ($\hat{\bar{\boldsymbol{x}}}_d$). The vector $\hat{\boldsymbol{y}}_{p,0}$ is defined such that it is contained in the global horizontal plane formed by the vectors $\hat{\boldsymbol{x}}_g$ and $\hat{\boldsymbol{y}}_g$ (see the left of Figure 3), and $\hat{\boldsymbol{z}}_{p,0}$ is defined so as to complete the orthonormal basis. The initial plane frame is then

$$\hat{\boldsymbol{x}}_{p,0} = \hat{\bar{\boldsymbol{x}}}_d,\ \boldsymbol{x}_{\text{temp}} = \bar{\hat{\boldsymbol{x}}}_d - (\bar{\hat{\boldsymbol{x}}}_d \cdot \hat{\boldsymbol{z}}_g)\hat{\boldsymbol{z}}_g,\ \hat{\boldsymbol{y}}_{p,0} = \boldsymbol{R}_z(\pi/2)\boldsymbol{x}_{\text{temp}}/||\boldsymbol{x}_{\text{temp}}||,\ \hat{\boldsymbol{z}}_{p,0} = \hat{\boldsymbol{x}}_{p,0} \times \hat{\boldsymbol{y}}_{p,0} \tag{1}$$

where $\boldsymbol{R}_z(\pi/2)$ is the transformation that performs a rotation around the z_g axis by an angle $\pi/2$; $\bar{\hat{\boldsymbol{x}}}_d$ is the time-filtered value of the instantaneous rotor-disk normal vector, $\boldsymbol{x}_d$; and $\boldsymbol{x}_{\text{temp}}$ is an intermediate variable.

The inflow velocity at the disk, $\boldsymbol{V}_w$, and the normal to the disk are used to define the skew coordinate system (x_s, y_s, z_s), the skew angle, χ_s, and the skew azimuthal angle, ψ_s. In a case with yaw and no tilt, the skew angle is the absolute value of the yaw angle, and $\psi_s = 0$ or $\psi_s = \pi$, depending on the sign of the yaw angle. In a case with tilt and no yaw, the skew angle is the absolute value of the tilt angle, and $\psi_s = \pm\pi/2$. In the general case, Figure 3 is used to define the skewed coordinate system and variables. The vector $\hat{\boldsymbol{x}}_s$ is set to $\hat{\bar{\boldsymbol{x}}}_d$. The vector $\hat{\boldsymbol{y}}_s$ is set in the plane formed by the wind speed and the disk normal, and the vector $\hat{\boldsymbol{z}}_s$ follows to form an orthonormal basis.

We define the meandering frame of reference as the frame in which all the wake planes are aligned such that the vectors of their respective frames are collinear. The planes in the global frame shown in Figure 2 are plotted in the corresponding meandering frame in Figure 4. The frame is simply noted with the coordinates x, y, z, without subscript.

In this frame the wake planes do not meander, and they only convect along the $\hat{\boldsymbol{x}}$ direction. The projection of the convection velocity of each plane in the axial direction is $U_i(\boldsymbol{p}_i) = \boldsymbol{V}_{c,i} \cdot \boldsymbol{x}_{p,i}$. In Figure 4, the wake planes at a given time t and at the next time step ($t + dt$) are shown, illustrating the re-indexing that occurs at the end of each time step (plane 0 becomes plane 1, carrying over its orientation and wake deficit, and so forth for

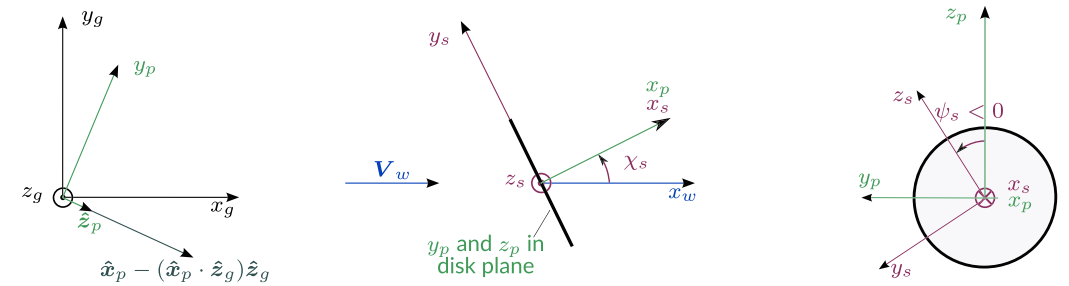

FIGURE 3 Definition of the wake plane and skew coordinate systems. These systems are determined for the initial plane ($i = 0$). The subscript 0 is dropped on the figure

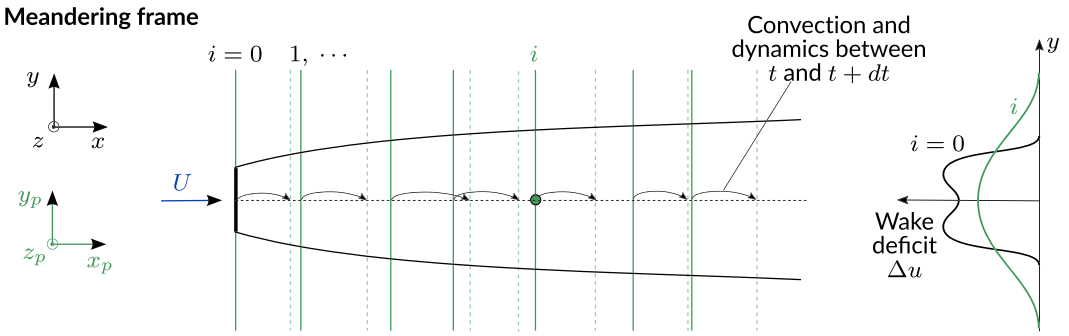

FIGURE 4 Wake planes in the meandering frame, as used in the module WakeDynamics. The meandering frame is such that all the wake planes frame are parallel and the wake centerline collapses to a straight line. The green solid lines are the plane locations at time t and the dashed green lines are the plane locations at $t + dt$

[†]We note that FAST.Farm does not support a coordinate system where the disk normal is vertical.

other indices). The indexing algorithm discards planes above a given index to limit the memory impact. In the following description, we will temporarily drop the index notation and use a continuous formulation before reintroducing it in Section 2.4.

We write $U(x)$ the convection velocity of each plane along the x coordinate of the meandering frame (x is the axial position of a wake plane expressed in a continuous way). The velocity field in the meandering frame of the wake of an isolated turbine (as is the case for the WakeDynamics module) is assumed to comprise the sum of the local convection velocity and a wake deficit contribution:

$$u = U + \Delta u, \quad v = V + \Delta v, \quad w = W + \Delta w, \tag{2}$$

where u, v, and w are the total velocity. The cross-flow velocities V and W are used by WakeDynamics to convect the planes; however, in the meandering frame, they are assumed to be zero. We now proceed to describe the original FAST.Farm and new curled wake formulations. The main differences between the formulations lie in the flow equations, the eddy viscosity model, and the initial wake deficit. The convection and time filtering are identical in both models.

2.2 | Original FAST.Farm formulation

Key elements of the FAST.Farm formulation are given below. The reader is referred to the FAST.Farm manual[19] for additional details.

2.2.1 | Flow equations

The original WakeDynamics formulation uses polar coordinates. The evolution of the wake deficits in the meandering frame of reference is obtained by solving the thin shear-layer approximation of the Reynolds-averaged Navier–Stokes equations under quasi-steady-state conditions and axisymmetric coordinates and by using an eddy viscosity formulation for the turbulence closure. From the axisymmetric assumption, the variables in each plane are stored along a radial line denoted with the coordinate r. The flow equations solved are the momentum and conservation of mass equations:

$$\frac{\partial u}{\partial t} u + u \frac{\partial u}{\partial x} + u_r \frac{\partial u}{\partial r} = \frac{1}{r} \frac{\partial}{\partial r} \left[r \nu_T \frac{\partial u}{\partial r} \right] \tag{3}$$

$$\frac{\partial u}{\partial x} + \frac{1}{r} \frac{\partial (r u_r)}{\partial r} = 0 \tag{4}$$

where u_r is the radial velocity and ν_T is the turbulent eddy viscosity, defined in Section 2.2.2. We have written the equations using a Eulerian formulation to ease the comparison with the curled wake formulation. We note that in the FAST.Farm manual, the equations are written in a Lagrangian formulation, and, under the quasi-steady assumption, the total derivative is reduced to only convection. We discuss the link between the Eulerian and Lagrangian formulations in Section 2.4. The equations are solved jointly using a second-order accurate implicit Crank–Nicolson scheme and second-order accurate central differences for the spatial derivatives.

2.2.2 | Eddy viscosity model

The eddy viscosity is computed at each coordinate of a wake plane as the sum of contributions from ambient turbulence and the wake shear layer:

$$\nu_T(x, r) = \max\left(\nu_{\text{amb}}(x), \nu_{\min}\right) + \nu_{\text{shr}}(x, r) \tag{5}$$

where we introduced a minimum viscosity term on the ambient viscosity inspired by the curled wake model,[11] and the different terms are expressed as

$$\nu_{\min} = 10^{-4} \overline{D} \bar{U}_w \tag{6}$$

$$\nu_{\text{amb}}(x) = F_{\text{amb}}(x) k_{\text{amb}} \overline{\text{TI}}_{\text{amb}} \bar{U}_w \frac{\overline{D}}{2} \tag{7}$$

$$\nu_{\text{shr}}(x,r) = F_{\text{shr}}(x) k_{\text{shr}} \max\left\{ l^{*2}(x) \left| \frac{\partial u(x,r)}{\partial r} \right|, l^{*}(x) u_{\min}(x) \right\} \tag{8}$$

The terms $F_\bullet$ are filters that depend on the downstream distance, the terms $k_\bullet$ are user scaling factors, l^* is a characteristic length scale of the wake size (taken as the rotor radius or computed based on the wake deficit), $\overline{\text{TI}}_{\text{amb}}$ is the time-filtered ambient turbulence intensity, $\bar{U}_w$ is the time-filtered disk average wind velocity normal to the actuator disk, $\overline{D}$ is the time-filtered rotor diameter velocity (changing due to elastic motion of the blades), and $u_{\min}$ is the minimum axial velocity at the current wake plane.

2.2.3 | Initial wake deficit

The first wake plane is emitted at the rotor location, and the initial wake deficit is set based on the time-filtered thrust coefficient ($\overline{C}_t$), obtained using the azimuthal average of the thrust force over the different blades. The total thrust coefficient, $\overline{C}_T$, is obtained by integrating the local thrust coefficient, C_t, with an appropriate radial weighting. Under low-thrust conditions ($\overline{C}_T < 24/25$), the initial induced velocity of the wake planes is

$$\Delta u(x=0, r_w) = -\bar{U}_{\text{rel}} C_{\text{NW}} \bar{a}(r), \quad \bar{a}(r) = \frac{1}{2}\left[1 - \sqrt{1 - \overline{C}_t(r)}\right], \quad r_w = r_w(r, \bar{a}(r)) \tag{9}$$

where r and r_w are the radii along the same streamline at the rotor and the wake, respectively, $\bar{U}_{\text{rel}}$ is the time-filtered rotor-disk-averaged relative wind speed ("relative" because it contains rotor elastic motion), C_{NW} is a tuning constant for the near wake (with a default value of $C_{\text{NW}} = 1.8$), and $\bar{a}(r)$ is the radially dependent induction, which is derived from $\overline{C}_t$, and $\overline{C}_t$ is bounded to an upper value of 24/25. Strip theory[‡] and conservation of mass are used to relate the radii r and r_w using $\bar{a}(r)$ and assuming that r_w is the end radius that would be obtained from strip theory. The induced velocity under mid- to high-thrust conditions is the topic of previous work.[23]

2.3 | Curled wake formulation

2.3.1 | Flow equations

The curled wake model is not axisymmetric, and a Cartesian coordinate system is used to describe the flow equations. Each plane comprises a regular grid of points in the y_p and z_p directions (see Figure 5). Only the momentum equation for the u component is solved for. Neglecting the pressure gradient, and in the absence of body force, it is approximated as

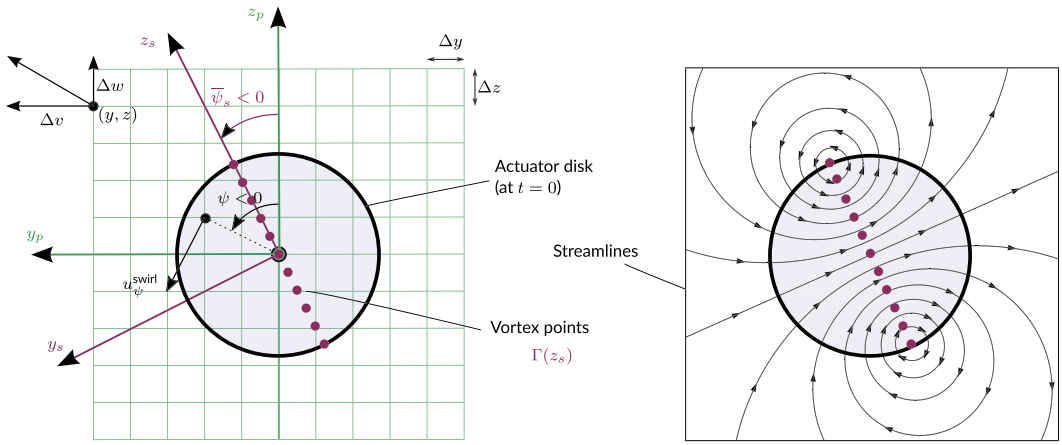

FIGURE 5 Schematic of Cartesian wake planes introducing the relevant notations for the curled wake formulation (left) and the resulting spanwise vectors from the curled wake model (right)

[‡]In this work, we use the term strip theory to refer to the 2D momentum theory with independence of annuli.[22]

$$\frac{\partial u}{\partial t}+u\frac{\partial u}{\partial x}+v\frac{\partial u}{\partial y}+w\frac{\partial u}{\partial z}=\frac{\partial}{\partial y}\left[\nu_T\frac{\partial u}{\partial y}\right]+\frac{\partial}{\partial z}\left[\nu_T\frac{\partial u}{\partial z}\right] \tag{10}$$

where ν_t is provided in Section 2.3.2. The right-hand side is an approximation of the divergence of the stress tensor. To obtain this term, we write f^{eddy} the divergence of the stress sensor, develop its expression, and perform some approximations as follows:

$$f^{\text{eddy}}=\frac{\partial}{\partial x_j}\left[\nu_T\left(\frac{\partial u_j}{\partial x}+\frac{\partial u}{\partial x_j}\right)\right]=\nu_T\nabla^2 u+2\frac{\partial u}{\partial x}\frac{\partial \nu_T}{\partial x}+\left[\frac{\partial v}{\partial x}+\frac{\partial u}{\partial y}\right]\frac{\partial \nu_T}{\partial y}+\left[\frac{\partial u}{\partial z}+\frac{\partial w}{\partial x}\right]\frac{\partial \nu_T}{\partial z}\approx\frac{\partial}{\partial y}\left[\nu_T\frac{\partial u}{\partial y}\right]+\frac{\partial}{\partial z}\left[\nu_T\frac{\partial u}{\partial z}\right] \tag{11}$$

where the first equality is the definition of the divergence of the stress sensor (using implied summation on the index j and the eddy viscosity ν_T), the second equality uses the continuity equation and the definition of the Laplacian (∇^2), and the last approximation assumes that the gradients along x are negligible. The approximation of f^{eddy} is used in the right-hand side of Equation (10). The curled wake model includes v and w components that are not obtained using continuity but are obtained based on the initial wake-induced velocity (see Section 2.3.3). An optional exponential decay is implemented on these components.[24] Details on the numerical implementation are provided in Section 2.4.

2.3.2 | Eddy viscosity model

In the curled wake formulation, the eddy viscosity ν_T is computed as the sum of the shear layer and ambient contributions, similar to Equation (5). The main difference is that it has to be computed on the Cartesian grid using Cartesian coordinates. Equation (7) is unchanged, but Equation (8) is modified as follows:

$$\nu_{\text{shr}}(x,y,z)=F_{\text{shr}}(x)k_{\text{shr}}\max\left\{l^{*2}(x)\left[\left|\frac{\partial u(x,y,z)}{\partial r}\right|+\left|\frac{1}{r}\frac{\partial u(x,y,z)}{\partial \theta}\right|\right],l^*(x)u_{\min}(x)\right\} \tag{12}$$

where the polar gradients are computed from the Cartesian variables as

$$\frac{\partial u}{\partial r}(x,y,z)=\frac{\partial u}{\partial y}(x,y,z)\frac{y}{r}+\frac{\partial u}{\partial z}(x,y,z)\frac{z}{r} \tag{13}$$

$$\frac{\partial u}{\partial \theta}(x,y,z)=-\frac{\partial u}{\partial y}(x,y,z)z+\frac{\partial u}{\partial z}(x,y,z)y \tag{14}$$

with $r=\sqrt{y^2+z^2}$, $\frac{\partial u}{\partial r}=0$, and $\frac{\partial u}{\partial \theta}=0$ when $r=0$. The total eddy viscosity is eventually given by

$$\nu_t(x,y,z)=\max\{\nu_{\text{amb}}(x),\nu_{\min}\}+k_{\text{curl}}\nu_{\text{shr}}(x,y,z) \tag{15}$$

where k_{curl} is a scaling factor introduced so that the curled wake model and the original formulation display similar diffusion without the need to recalibrate k_{shr} constants of FAST.Farm.[17] The adjusted eddy viscosity is used to compensate for the missing terms in the equations, in particular, the lack of continuity.[17] We discuss and tune the constant k_{curl} in Section 3.1, where we found that values between 1.4 and 3 gave satisfactory results.

2.3.3 | Initial wake deficit

The axial component of the initial wake (Δu at $x=0$) is obtained using Equation (9). In the curled wake formulation, cross-flow components are present, unlike in the original formulation (other than δu_r, which is derived from continuity). The cross-flow components are obtained as the sum of induced velocities coming from the wake swirl and the curled wake.

$$\Delta v=\Delta v^{\text{curl}}+\Delta v^{\text{swirl}},\quad \Delta w=\Delta w^{\text{curl}}+\Delta w^{\text{swirl}} \tag{16}$$

The notations used for the velocities defined in plane are given in Figure 5. We obtain the tangential swirl-induced velocity from strip theory:

$$u_{\psi}^{\text{swirl}}(r_w) = C_{\text{NW}}\overline{C}_q(r)\frac{\bar{U}_{\text{rel}}}{4[1-\bar{a}(r)]}, \quad r_w = r_w(r, \bar{a}(r)) \tag{17}$$

where the relationship between r and r_w is the same as that used in Equation (9), $\overline{C}_q$ is the time-filtered and azimuthally averaged local torque coefficient, and Equation (17) is valid up to thrust coefficients $\overline{C}_t(r) = 24/25$ (where $\bar{a}(r) = 0.4$). For high thrust coefficients ($C_T > 1.1$), the swirl is disabled ($u_{\psi}^{\text{swirl}}(r_w) = 0$). The swirl-induced velocities are directly obtained by projecting the tangential velocity:

$$\Delta v^{swirl}(y,z) = u_{\psi}^{swirl}(r)\frac{z}{r}, \quad \Delta w^{swirl}(y,z) = -u_{\psi}^{swirl}(r)\frac{y}{r} \tag{18}$$

The curled-wake-induced velocities are obtained similarly to the original curled wake formulation.[11] In the original curled wake formulation, the curled vortices are along $\hat{\boldsymbol{x}}_w$, whereas they are placed along $\hat{\boldsymbol{x}}_p$ in the FAST.Farm formulation. This choice was made for convenience and is expected to have limited influence on the results for moderate yaw angles. In the general context of FAST.Farm, both yaw and tilt will skew the wake. Each plane is attributed a skewed coordinate system at initialization based on the skew angle formed between the average wind at the rotor disk and the normal to the disk. In the original curled wake model, infinite vortices are distributed along the vertical ($\psi_s = 0$) to obtain cross-flow components for a rotor in yaw. In the general case, the infinite vortices are titled based on the azimuthal angle $\overline{\psi}_s$ such that they are passing through the rotor plane at the locations $y_0 = -z_s \sin\overline{\psi}_s$ and $z_0 = z_s \cos\overline{\psi}_s$ in the plane coordinate system, with $z_s \in [-R; R]$, and $R = \overline{D}/2$ is the filtered rotor radius (see Figure 5). The induced velocity in the first wake plane is then obtained from the Biot–Savart law as

$$\Delta v^{curl}(y,z) = \int_{-R}^{R} V_{\sigma}(y-y_0, z-z_0)\frac{\Gamma z_s}{R\sqrt{R^2-{z_s}^2}}dz_s, \quad \Delta w^{curl}(y,z) = \int_{-R}^{R} W_{\sigma}(y-y_0, z-z_0)\frac{\Gamma z_s}{R\sqrt{R^2-{z_s}^2}}dz_s \tag{19}$$

where the regularized kernels of the Biot–Savart law are given by:

$$V_{\sigma}(y,z) = \frac{-z}{2\pi r^2}\left[1-e^{-r^2/\sigma^2}\right], \quad W_{\sigma}(y,z) = \frac{y}{2\pi r^2}\left[1-e^{-r^2/\sigma^2}\right] \tag{20}$$

The regularization parameter, σ, is chosen as $\sigma = 0.2\overline{D}$. The circulation is computed as[16,17]

$$\Gamma = \frac{\overline{D}}{2}\bar{U}_{\text{rel}}\overline{C}_T \sin\overline{\chi}_s \cos\overline{\chi}_s \tag{21}$$

where $\overline{\chi}_s$ is the time-filtered skew angle. The numerical integration used in Equation (19) is performed using the midpoint rule based on a number of points specified by the user (100 points by default).[11] In the FAST.Farm implementation, a decay is introduced on the velocities obtained, as discussed in the following section.

2.4 | Implementation details

To implement the curled wake algorithm described in Section 2.3, several changes had to be introduced to the WakeDynamics and AWAE modules and to the OpenFAST wrapper.

2.4.1 | OpenFAST wrapper

The changes to the OpenFAST wrapper are as follows:

- The actuator disk torque coefficient, $C_q(r)$, is now computed together with the thrust coefficient, $C_t(r)$, and passed to WakeDynamics to compute the swirl-induced velocities (see Equation (17)).
- The instantaneous skew angle, χ_s, and skew azimuthal angle, ψ_s, are computed and passed to WakeDynamics to compute the skew coordinate system (see Figure 3).

2.4.2 | AWAE module

The changes to the AWAE module are as follows:

- Previously, the module took as inputs the induced velocities at each wake location in polar coordinates (Δu and Δu_r) and on radial lines. The module now receives the induced velocities in Cartesian coordinates (Δu, Δv, Δw) and on 2D planes (in the y–z directions). This update applies to both the curled wake and polar formulations.
- The internal algorithms of AWAE that merge wakes and interpolate the full velocity fields (made of wakes and background flows) at requested locations were adapted to use the new Cartesian inputs. To introduce these changes, we compute the coordinate systems of each plane (x_p, y_p, z_p) according to Equation (1), and we introduce a 2D interpolation algorithm to interpolate quantities between two 2D planes.
- We introduced a new option to AWAE to remove the wake deficits that are transverse to the local ambient flow direction from the calculation of the wake plane meandering velocities that are an output of AWAE. That is, the contribution of the velocity deficits across the plane (Δu, Δv, Δw) that is transverse to the local flow is neglected when calculating the spatial average of the disturbed (ambient plus wakes) wind velocity across the plane, which is used to meander the plane. By default, this option is active with the curled wake model, and inactive otherwise. This feature avoids a double counting of the convection in the transverse direction because the curled wake algorithm in WakeDynamics already accounts for this convection. For the original polar formulation, the transverse component of the deficit is important for capturing deflection of the wake from a rotor that is skewed relative to the inflow.

2.4.3 | WakeDynamics module

The changes to the WakeDynamics module are as follows:

- We changed the outputs of WakeDynamics such that the module always returns velocities in Cartesian coordinates and on 2D planes, thereby matching the new input convention of AWAE discussed above. This update applies to both the curled wake and polar formulations. The main change affects the polar formulation, where the axisymmetric velocities $\Delta u(r)$ and $\Delta u_r(r)$ are projected onto Cartesian values ($\Delta u(y,z)$, $\Delta v(y,z)$, $\Delta w(y,z)$) as follows:

$$\Delta u(y,z) = \Delta u(r), \quad \Delta v(y,z) = \Delta u_r(r)\frac{y}{r}, \quad \Delta w(y,z) = \Delta u_r(r)\frac{z}{r} \tag{22}$$

  where $r = \sqrt{y^2+z^2}$, and the cross-flow components are zero when $r = 0$. In the curled wake formulation, the Cartesian coordinates on the Cartesian planes are already the main variables. Additional outputs were added to FAST.Farm to write to disk the different information stored in each wake plane, such as velocity deficit and eddy viscosity.

- The update of states now contains different implementations, whether the curled wake formulation or polar formulation is used. We describe the former in the following. The velocity deficit of the initial wake plane is set according to Section 2.3.3. The inclusion of swirl velocities is an option available to the user. WakeDynamics uses a Lagrangian convection of the planes. The wake positions are updated as follows:

$$\frac{dx_p}{dt} = U + \Delta u \tag{23}$$

  where d/dt is the material derivative associated with the convection with the background flow, U:

$$\frac{d}{dt} = \frac{\partial}{\partial t} + (U+\Delta u)\frac{\partial}{\partial x} \tag{24}$$

  We note that the true material derivative is

$$\frac{D}{Dt} = \frac{\partial}{\partial t} + (U+\Delta u)\frac{\partial}{\partial} + (V+\Delta v)\frac{\partial}{\partial y} + (W+\Delta w)\frac{\partial}{\partial z} = \frac{d}{dt} + \Delta u\frac{\partial}{\partial x} + \Delta v\frac{\partial}{\partial y} + \Delta w\frac{\partial}{\partial z} \tag{25}$$

  We implement the update of states from time t to $t+dt$ (from time step n_t to n_t+1) by updating the states of the plane with index $i-1$ to the ones with index plane i. Therefore, the discrete form of Equation (23) is implemented using a first-order forward Euler scheme as

$$x_{p,i}[n_t+1] = x_{p,i-1}[n_t] + U_{i-1}[n_t]\Delta t \tag{26}$$

where brackets are used to indicate the time step at which the variable is evaluated. Equation (26) is the same for the polar and curled wake formulations. Because the background flow in the meandering frame is constant and is laterally uniform, Equation (10) becomes

$$\frac{\partial U+\Delta u}{\partial t} + (U+\Delta u)\frac{\partial (U+\Delta u)}{\partial x} + \Delta v\frac{\partial \Delta u}{\partial y} + \Delta w\frac{\partial \Delta u}{\partial z} = \frac{\partial}{\partial y}\left[\nu_T\frac{\partial \Delta u}{\partial y}\right] + \frac{\partial}{\partial y}\left[\nu_T\frac{\partial \Delta u}{\partial z}\right] \tag{27}$$

Using Equation (24), Equation (27) becomes the following mixed Eulerian–Lagrangian formulation:

$$\frac{d\Delta u}{dt} + \Delta v\frac{\partial \Delta u}{\partial y} + \Delta w\frac{\partial \Delta u}{\partial z} = \frac{\partial}{\partial y}\left[\nu_T\frac{\partial \Delta u}{\partial y}\right] + \frac{\partial}{\partial y}\left[\nu_T\frac{\partial \Delta u}{\partial z}\right] \tag{28}$$

We discretize Equation (28) using a first-order forward scheme as follows:

$$\Delta u_i[n_t+1] = \Delta u_{i-1}[n_t] + \Delta t\left[-\Delta v_{i-1}[n_t]\frac{\partial \Delta u_{i-1}[n_t]}{\partial y} - \Delta w_{i-1}[n_t]\frac{\partial \Delta u_{i-1}[n_t]}{\partial z} + f^{\text{eddy}}_{i-1}[n_t]\right] \tag{29}$$

where f^{eddy} is the term on the right-hand side of Equation (27). All the gradients are computed using a central-difference scheme. We use an optional exponential decay on the cross-flow components of the planes,[24] which is implemented as

$$\Delta v_i[n+1] = \Delta v_{i-1}[n]e^{-k_{vd}\Delta x/D} \tag{30}$$

$$\Delta w_i[n+1] = \Delta w_{i-1}[n]e^{-k_{vd}\Delta x/D} \tag{31}$$

with $\Delta x = U_{n_p-1}[n_t]\Delta t$. The decay is used to reduce the intensity of the vortices and effectively diffuse them downstream. We recommend the value $k_{vd} = 0.1$, which is such that the vortices have decays by 50% of their strength at a downstream distance of 7 rotor diameters, or 7*D*.

2.5 | Summary of main differences

We conclude this section by listing the main differences between the polar and curled wake formulations in Table 1.

3 | RESULTS

In this section, we verify the implementation of the curled wake formulation by comparing it with the polar formulation and with actuator line and actuator disk large-eddy simulations (LES). In all cases, we use the NREL 5-MW baseline wind turbine.[25] The tilt is set to zero, and the turbine is rigid and operating at a constant rotational speed, unless mentioned otherwise. All simulations use the calibrated constants $k_{\text{curl}} = 2$ (for the eddy viscosity) and $f_c = 0.018$ Hz (for the time filter), unless mentioned otherwise.

3.1 | Uniform inflow with aligned rotor

We start the verification of the curled wake formulation by considering a case with steady, uniform inflow. We run a simulation for a uniform wind of velocity $U = 8$ m/s and a rotor speed of $\Omega = 12.1$ rpm, corresponding to $C_T = 0.72$ and $\lambda = 6.5$. The swirl is not included in these simulations to minimize the differences between the two formulations. We note that cases with uniform inflow are challenging because FAST.Farm was designed and tuned[26] to be used with turbulent simulations where the ambient turbulent effects on the convection and diffusion are the most important. We compare the wake velocity deficits at three downstream locations, $x = \{1, 5, 8\}D$, in Figure 6.

In this case (without yaw), the two formulations (polar, curl) are expected to return similar results. The main sources of differences are the numerical scheme, the handling of continuity, and the scaling factor used in the eddy viscosity (see Table 1). The differences in wake shapes downstream are likely to be attributed to the fact that the curled wake model does not account for continuity, resulting in a different wake expansion. Overall, the agreement appears to be satisfactory in light of the differences in formulations.

TABLE 1 Differences between the polar and curled wake formulations in WakeDynamics

Feature	Polar (FAST.Farm)	Curl (FAST.Farm)	Curl (original)
Time formulation	quasi-steady	quasi-steady	steady
Equation formulation	Eulerian/Lagrangian	Eulerian/Lagrangian	Eulerian
Frame	meandering ($x = x_p$)	meandering ($x = x_p$)	global ($x = x_g$)
Coordinate system	polar	Cartesian	Cartesian
Plane points	radial line	2D grid	2D grid
Continuity equation	included	not included	not included
Eddy viscosity	ambient + shear (radial)	idem but with $\frac{\partial u}{\partial \theta}$ and scaling factor	constant based on mixing length
Momentum equation	shear layer approx.	idem but in Cartesian	idem
Numerical scheme	implicit Crank–Nicolson	first-order forward Euler	idem
Lagrangian convection	U may contain cross-flow	U does not contain cross-flow	–
Wake lateral convection	deflection model[a]	modified deflection model[b] +intrinsic	intrinsic
Initial deficit	axial, based on C_t	idem, but with swirl and curl cross-flows	idem but no swirl
Curled vortices	–	distributed along $\hat{\mathbf{z}}_s$ in $\hat{\mathbf{x}}_p$ direction	distributed along $\hat{\mathbf{z}}_g$ in $\hat{\mathbf{x}}_w$ direction
Wake superposition	root-sum-square	root-sum-square	–
Rotor loads	blade element momentum	blade element momentum	Look-up table
Secondary steering	–	intrinsic	intrinsic

Note: "Idem" indicates that the value is the same as the previous column.
[a]The lateral deflection depends on the velocity deficit transverse to the local flow.
[b]The parameters are adapted to account for the intrinsic convection already present.

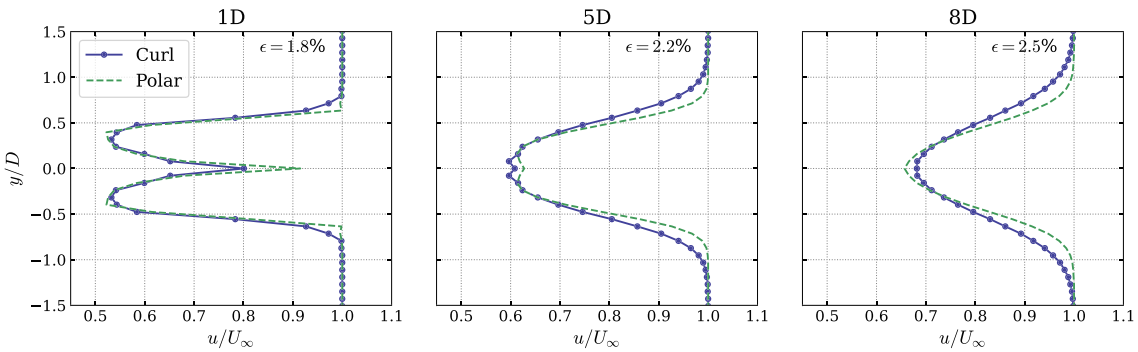

FIGURE 6 Wake velocity deficits for a case with uniform inflow and aligned rotor as obtained by the different FAST.Farm formulations. The relative error, ϵ, between the two curves, is indicated on the figure

In Figure 6 we obtained a similar diffusion of the wake by tuning the eddy viscosity constant of the curled wake model, obtaining $k_{\text{curl}} = 2$. We performed a sensitivity analysis and found no dependency of this scaling factor on the time step and grid size. As mentioned in Section 2.3.2, the scaling constant likely comes as a result from the lack of continuity in the curled wake formulation. The velocity gradients obtained at the wake boundary are smaller in the curled wake formulation, leading to smaller values of ν_{shr} before being scaled. The value we obtained is in line with the tuning constant found in previous studies.[17]

We repeated this study for different thrust coefficients and computed the relative error between the curl and polar wake deficits at 5*D*. For thrust coefficients of 0.4, 0.7, and 0.9, the relative error between the two formulations was 1%, 2.5%, and 6.4%, respectively, using $k_{\text{curl}} = 2$. With $k_{\text{curl}} = 2$, the curl formulation diffuses slightly too much for a low value of the thrust coefficient, and not enough for a high value of the thrust coefficient. The errors are reduced to 0.5%, 2.5%, and 5.1% using values of k_{curl} of 1.4, 2.0, and 3.0, respectively. We therefore recommend using these values as a function of the mean thrust coefficient of a given simulation.

3.2 | Turbulent inflow with aligned rotor

We build on the test case presented in Section 3.1 by adding turbulence to the simulation. FAST.Farm is mostly intended to run cases with turbulent inflow where the wake effectively meanders. The turbulent inflow was generated with TurbSim[27] using the Kaimal spectrum, a turbulence intensity of 13.3%, a power law coefficient of 0.2, and recommended spatial coherence functions. The operating conditions are $U = 8.09$ m/s and $\Omega = 9.16$ rpm, corresponding to $C_T = 0.80$ and $\lambda = 7.43$. The nacelle yaw angle is kept at zero, but because of the turbulent inflow, a nonzero skew angle is present, ranging from 0° to ± 12°, therefore activating the cross-flow velocities from the curled wake vortices. The swirl effect is not activated to minimize the differences between the two formulations. We run 1-h simulation, based on a 1-h long turbulence box, and averaged the results over the last 3500 s. We plot the time-averaged wake velocity deficits (in the global frame) obtained using the different formulations at three downstream distances in Figure 7. For these simulations we found that the value $k_{\nu,\text{curl}} = 2.7$ was best to match the diffusion of both formulations.

The conclusions are similar to the ones presented in Section 3.1. The two formulations have a similar diffusion of the wake, but the wakes from the curled wake formulation expand more, likely due to the lack of continuity.

3.3 | Yawed inflow without swirl

In this section, we perform simulations with a constant yaw angle of 30 deg, under uniform inflow. For consistency with previous results shown in the literature, we use the test case from Martínez et al[11] and the LES actuator disk results from Howland et al.[9] For simplicity, the actuator disk models account only for the axial loads and not the tangential loads. Therefore, the effect of swirl is not included in the LES and FAST.Farm models. The operating conditions are $U = 12$ m/s and $\Omega = 8.4$ rpm, corresponding to $C_T = 0.55$ and $\lambda = 5.2$. We present simulation results for the original curled wake model (stand-alone Python implementation), the FAST.Farm models ("FF Curl" and "FF Polar"), and the LES actuator disk. The LES and Python models assume a uniform thrust distribution across the rotor, which will introduce differences in the wake deficit profiles because FAST.Farm uses a more realistic wind turbine model with rotor loading that is not uniform. We present the nondimensional axial velocity (u/U) and the cross-flow streamlines at different downstream locations behind the rotor in Figure 8.

From a qualitative inspection of the results, the FAST.Farm model appears to capture the underlying physics of a yawed-wake: the wake curls along the skewed wake axis, and cross-flow components analog to two counter-rotating vortices are present. These flow features are absent in the polar formulation because no cross-flow velocities are present. Small differences are observed between the stand-alone curl and FAST.Farm curl formulations, which are attributed to three factors, ordered by decreasing impact: (1) the stand-alone formulation uses a uniform thrust distribution, whereas the FAST.Farm formulation distributes the thrust (and induction) radially; (2) the curled vortices are along $\hat{\mathbf{x}}_p$ in the FAST.Farm formulation, whereas they are along $\hat{\mathbf{x}}_w$ in the stand-alone formulation; (3) the stand-alone formulation uses a different eddy viscosity formulation (using a uniform eddy viscosity across the plane).

There are visible differences between the LES results and the curled wake results. The LES simulations include the tower and use a uniform thrust distribution across the rotor. In general, it appears that the LES wake convects further in the skewed direction and the entire wake is transported, whereas the curled wakes display a lagging "tail" in the center of the wake that is not transported sufficiently fast.

To further illustrate the differences between the models, we plot the wake deficit along the horizontal line $z = 0$ (corresponding to the hub height) in Figure 9.

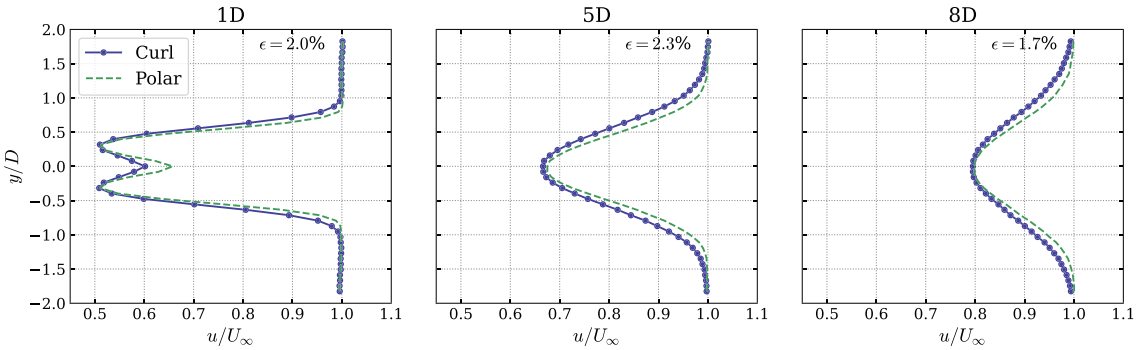

FIGURE 7 Average wake velocity deficits for a case with turbulent inflow and aligned rotor as obtained by the different FAST.Farm formulations

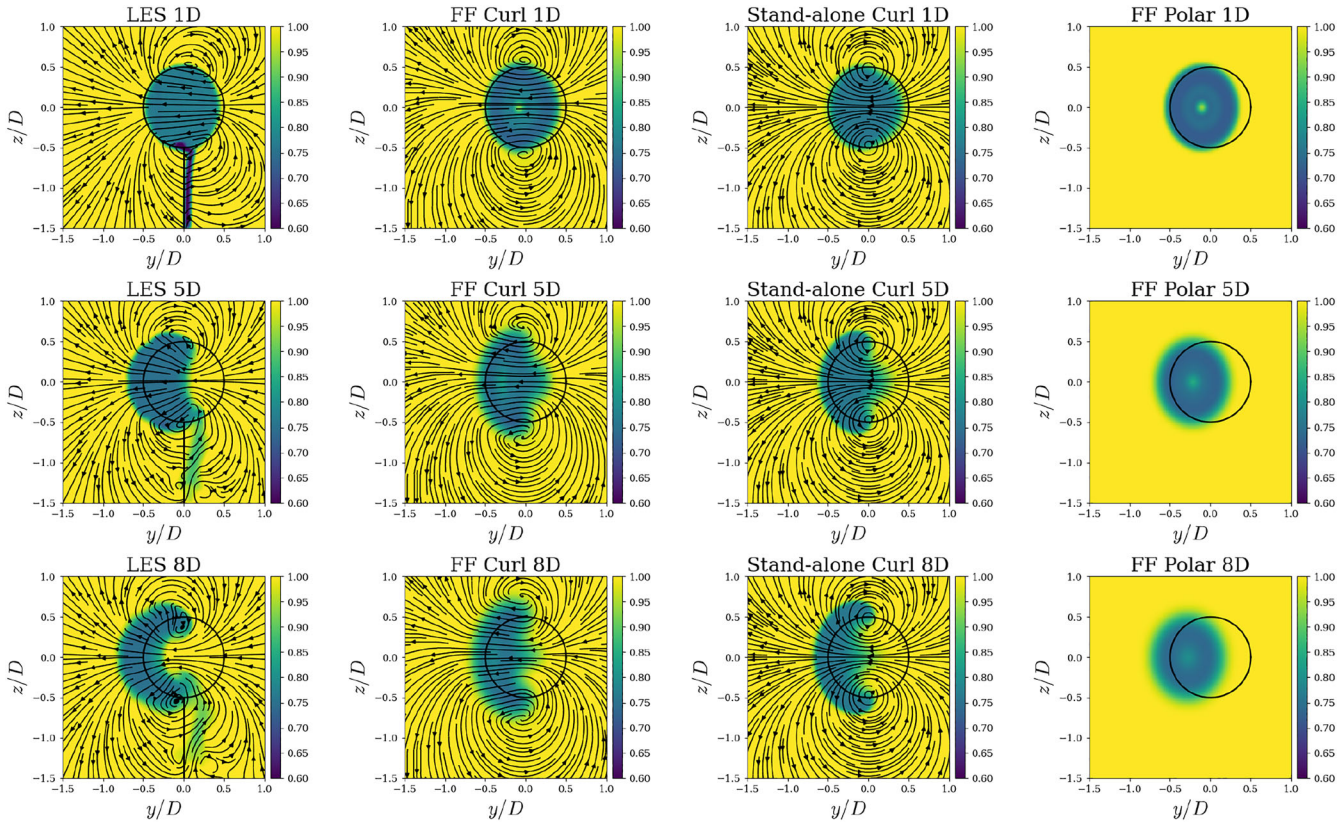

FIGURE 8 Nondimensional streamwise velocity contours of FAST.Farm curled wake model (FF Curl, left middle) compared to the LES results of an actuator disk model from Howland et al.[9] (left); results from the stand-alone curled wake model (right middle); and results from the FAST.Farm polar model (right). Streamlines show the cross-flow velocity components

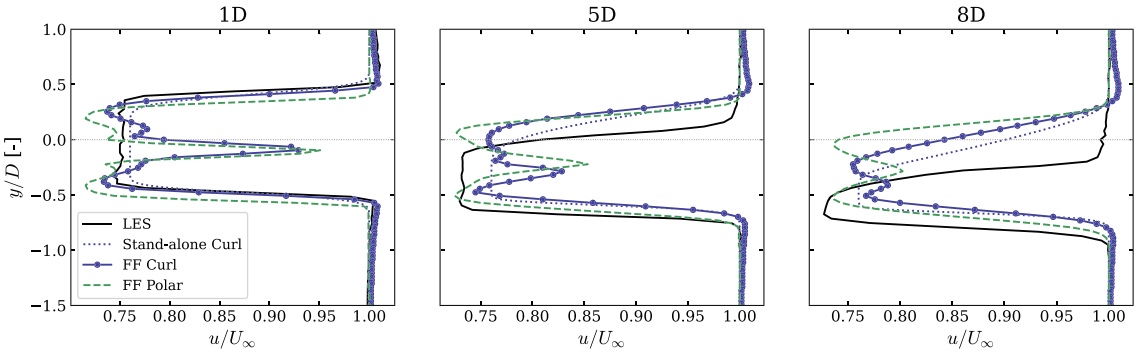

FIGURE 9 Wake deficits from Figure 8 extracted on the horizontal line $z = 0$ (hub height) at different downstream distances

The conclusions drawn from Figure 9 are similar to the ones mentioned above. The hub losses present in the FAST.Farm models are clearly visible on the figure. Though they are a source of the differences, we do not expect the difference in loading distribution to be the main contributor to the differences observed, as the stand-alone curl model (which has a uniform loading) displays similar behavior to the FAST.Farm curl model. In general, the engineering models are observed to deflect less (toward negative y) compared to the LES model. The polar model deflects with similar proportion as the other engineering models but keeps a symmetric wake deficit shape. Both curl models display asymmetric wake deficits at 8D, consistent with the LES results but with wider wake deficits.

Future improvements of the curled formulation might be possible by, for instance, changing the distribution of the vortex intensities such that the cross-flow transport is increased. The current distribution is equivalent to the distribution of a single vortex cylinder[18] (or constant thrust coefficient), and improvement might be possible by using a continuous distribution of circulation.[28]

3.4 | Yawed inflow with swirl

Here, we use the second test case previously presented for the curled wake model.[9,11] The operating conditions are $U = 8$ m/s and $\Omega = 7.5$ rpm, corresponding to $C_T = 0.75$ and $\lambda = 6.97$. Apart from the change in operating conditions, the main difference with Section 3.3 is that the effect of swirl is included for all simulations (except for the FAST.Farm polar model), and an actuator-line representation of the rotor is used for the LES case (and the tower is not included). We present velocity fields from the different formulations at different downstream locations in Figure 10.

For the results presented in Figure 10, the deflection parameters of FAST.Farm had to be changed so that the polar formulation deflects less[§] to match the other models. With the inclusion of swirl, the wake curls more in all simulations and the differences between the three methods are more pronounced. As before, the stand-alone curl assumes a uniform thrust distribution; therefore, the axial velocity is uniform at the rotor plane, whereas the other formulations display the usual reduction of axial induction at the rotor center due to important swirl and drag at this location. We believe this is the main source of the differences between the FAST.Farm and stand-alone curled wake formulations. The curled wake formulations qualitatively capture the flow behavior observed in the LES simulation, but the lateral transport is likely too weak and differences are observed in the way the deficit concentrates around the top vortex.

To further investigate the differences between the bottom and top vortices, we plot the wake deficits along the vertical line $y = 0$ in Figure 11.

We observe differences in the wake deficits at 1D between FAST.Farm and LES that likely originate from differences of loading at the rotor. At further distances downstream, the curling of the wake due to the swirl leads to a stronger wake deficit at the top of the wake (the concentration would be at the bottom for a negative yaw angle). This phenomenon is captured by the curl models but is clearly absent for the polar formulation. The FAST.Farm formulation displays wider wake deficits than the LES or stand-alone curl models, but the agreement is deemed satisfactory given the unavoidable errors introduced by the simplified engineering models.

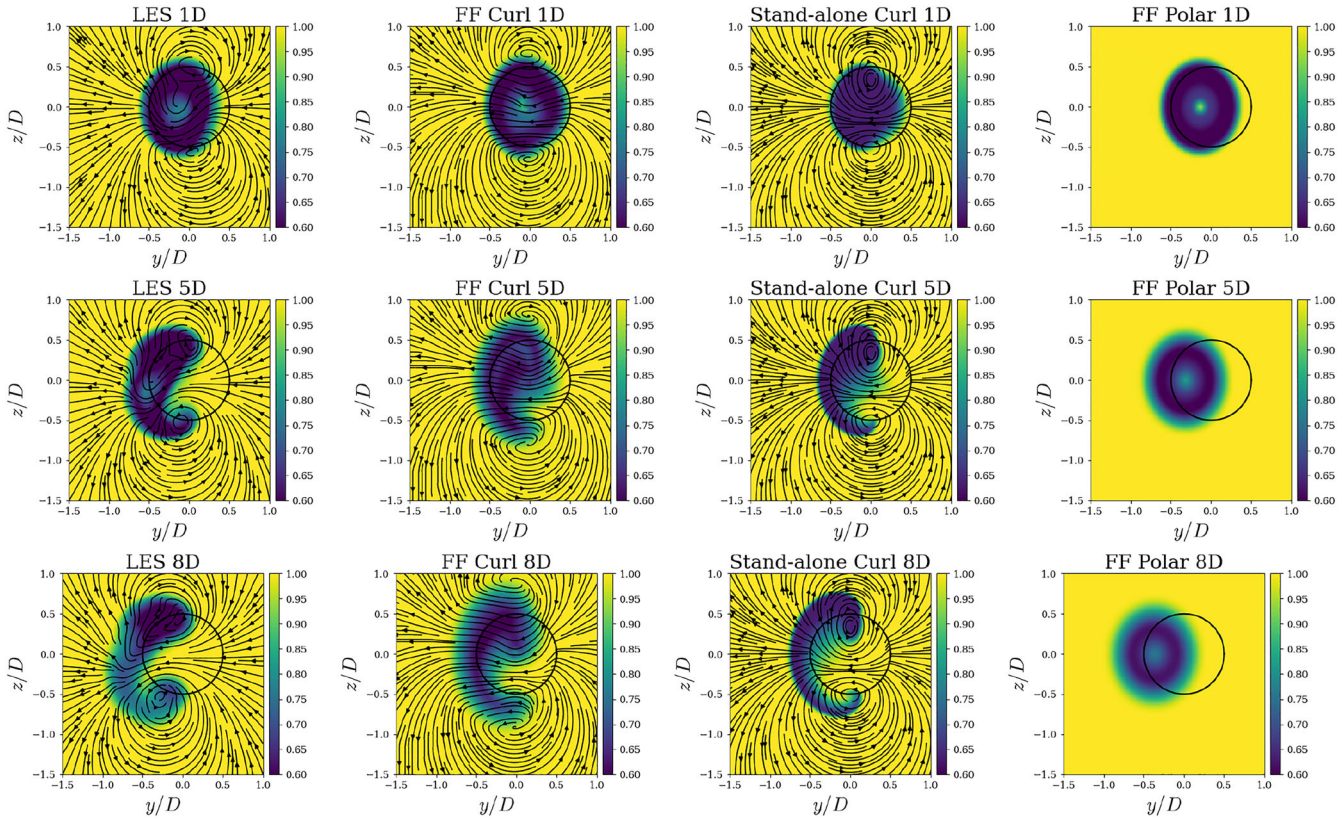

FIGURE 10 Nondimensional streamwise velocity contours of FAST.Farm curled wake model (middle left) compared to the LES results of an actuator line model from Howland et al.[9] (left), results from the stand-alone curled wake model (middle right) and results from the FAST.Farm polar formulation (right). The effect of swirl is included. Streamlines show the cross-flow velocity components

[§]There is an expected dependence on the deflection parameters of the FAST.Farm polar formulation with the thrust coefficient. It is noted that these deflection parameters are not used in the curled formulation.

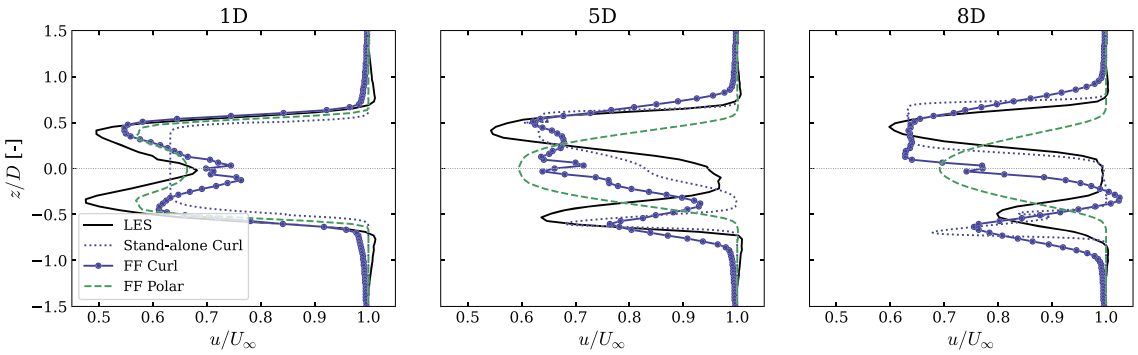

FIGURE 11 Wake deficits from Figure 10 extracted on the vertical line $y = 0$ at different downstream distances

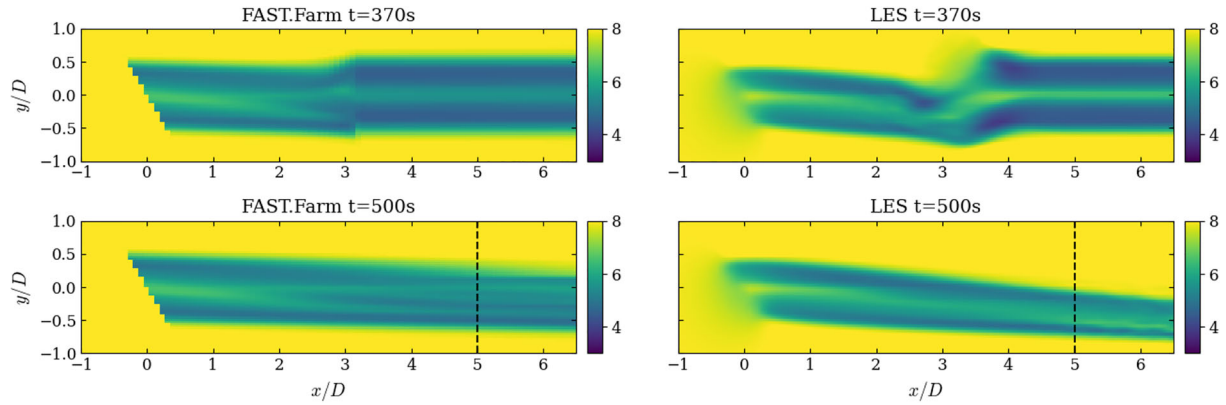

FIGURE 12 Snapshots of axial velocity as obtained by FAST.Farm (left) and LES (right) for a step-yaw event. At $t = 370$ s the transition between the uniform and yawed wake is at the middle of the domain. At $t = 500$ s, the yawed-wake is fully converged

3.5 | Transient response to a yaw step

We continue our verification by looking at a transient yaw event under uniform inflow. The operating conditions are: $U = 8$ m/s and $\Omega = 7.5$ rpm, corresponding to $C_T = 0.67$ and $\lambda = 6.5$. The rotor is initially aligned with the flow. At $t = 300$ s, the rotor is yawed from 0° to 30° over the span of 3 s. We use this test case to tune the time filter (mentioned in Section 2.1.2) used by WakeDynamics. The time filter effectively represents the dynamic inflow (also referred to as dynamic wake) effect,[22,29] which represents the time scale for changes of induction/circulation at the rotor to be propagated downstream, or similarly, the time for the vorticity to be convected downstream.[28] In order to tune this time constant, we simulated the transient yaw event under uniform inflow with FAST.Farm and an LES using the actuator line model.[30,31] We present snapshots of the wake axial velocity obtained with FAST.Farm and LES in Figure 12.

As seen from the LES results, a vortex is formed in the wake in the transition region between the uniform wake and the yawed wake as a result of the sudden yaw step. This vortex is similar to the vortex generated for a sudden pitching of an airfoil.[32] FAST.Farm does not have the necessary physics to fully capture such a phenomenon. We plot a cross section of the wake from LES and FAST.Farm at $x = 5D$ and $t = 500$ s in Figure 13. The cross section is indicated with dashed lines in Figure 12.

The results are consistent with the ones presented in Section 3.4.

To quantify the time evolution of the wake, we use an integral measure that compares the velocity field at one downstream plane (e.g., located at $x = 5D$) at the end of the simulation ($t = 600$ s), to the velocity field at the same downstream distance but at earlier times ($t < 600$ s). We use the mean relative error as a measure, and by definition this error is 0 at the end of the simulation. We do not expect this measure to be the same for both FAST.Farm and LES; therefore, we scaled it such that all simulations return the same error prior to the transient yaw event. The time evolution of this measure is shown in Figure 14.

The figures contain three main levels connected by transients: (1) the level prior to the wake reaching a given downstream location (as a result of the simulation start-up transients), (2) the level corresponding to the converged unyawed wake, (3) the final level corresponding to a converged yawed wake. We have scaled them such that level 2 is unity and level 3 is zero. The vortex that forms after the yaw step is visible at $x = 5D$ and

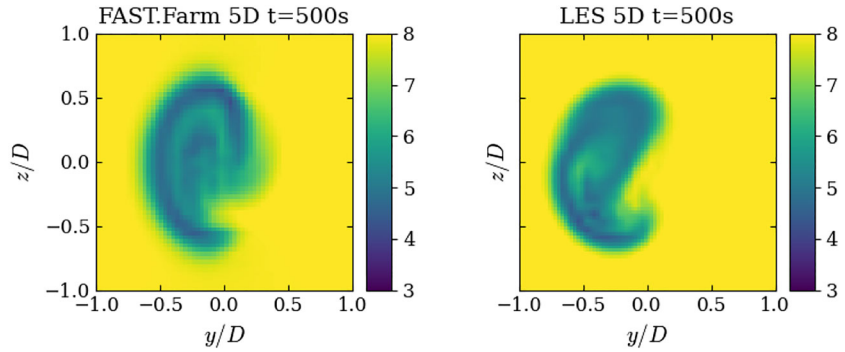

FIGURE 13 Instantaneous axial velocity from FAST.Farm and LES for the yawed wake, at $t = 500$ s, when the wake has converged

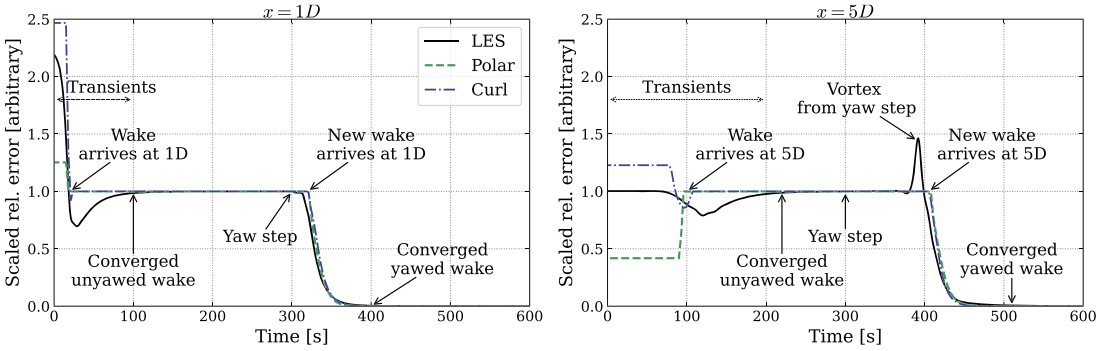

FIGURE 14 Integral measure representing the difference between the fully developed yawed wake and wakes at prior times for simulations of the transient event going from zero yaw to 30° yaw around $t = 300$ s. Left: values at $x = 1D$. Right: values at $x = 5D$

$t = 380$ s in Figure 14. The time constant from level 2 to level 3 is relevant for the dynamic wake effect and the constant f_c. For this simulation, we found that a filter frequency of $f_c = 0.18$ Hz provided results consistent between FAST.Farm and the LES results. This constant is different from the one recommended in previous work.[26] We believe that the previous calibration work missed the appropriate time scale by using an incomplete range for the calibration and focusing on average quantities (such as the wake position) during turbulent simulations. From our updated results, we suggest using a time filter that is consistent with the typical time scales used in dynamic inflow models:

$$\tau_1 = \frac{1.1}{1 - 1.3\min(a_{\text{avg}}, 0.5)}\frac{R}{U}, \quad f_c = \frac{2.4}{\tau_1} \tag{32}$$

where τ_1 is the time scale used in the Øye dynamic inflow model,[29] and a_{avg} is the average axial induction factor across the rotor disk (in our simulation, $a_{\text{avg}} = 0.25$).

3.6 | Sinusoidal yaw variations for two aligned turbines

In this section, we use the same test case as the one presented in Section 3.5, but we introduce an additional turbine, 7*D* downstream. The nacelle yaw angle of the first wind turbine (T1) is varied sinusoidally after time $t = 500$ s, with a period of $T = 250$ s. The rotational speed of the second turbine (T2) is fixed at $\Omega = 5.5$ rpm throughout the simulation. We compare the power of the turbines obtained using FAST.Farm and LES in Figure 15.

We observe that the power of T1 (and T2) oscillates at twice the frequency of the nacelle oscillation because the aerodynamic loads are nearly symmetric for positive and negative yaw. Differences in power levels are observed when the nacelle yaws, indicating that the yaw model of OpenFAST could likely be further improved. The power of the waked turbine shows strong 3p oscillations (where p is the frequency corresponding to the rotor speed) due to the sampling of the oscillating wake. The amplitude of the oscillations was reduced in the figure by applying a moving average filter of window length 1 s to help the readability and focus on the oscillations induced by the nacelle yaw. The LES and FAST.Farm results display different convection times of the wake. For the LES, the steady-state wake hits T2 later than the FAST.Farm

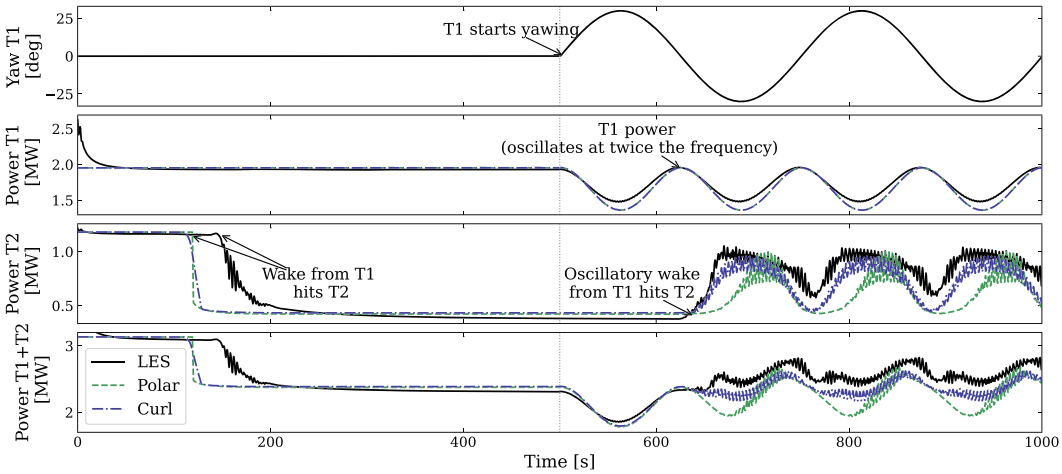

FIGURE 15 Response to a sinusoidal nacelle yaw variation of an upstream turbine (T1) on the downstream turbine (T2) as simulated using LES and FAST.Farm

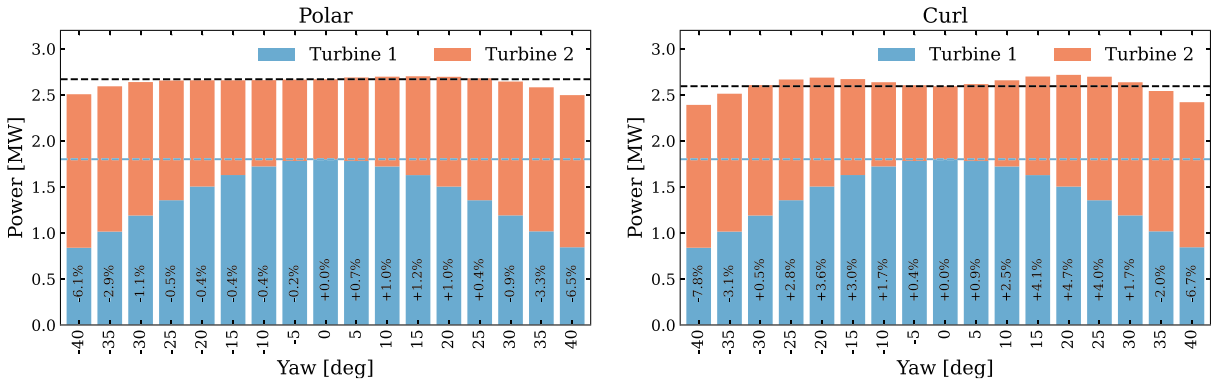

FIGURE 16 Power obtained for two turbines when the yaw angle of the first turbine is varied, obtained with the original (polar) and curled wake (curl) formulations. The percentage difference of the total power compared to the zero-yaw configuration is indicated on the figure

simulation, which is likely explained by the slow buildup of the wake and induction in LES, whereas FAST.Farm assumes that the axial induction of a fully developed wake is present at $t = 0$. The oscillatory wake hits T2 at approximately the same time ($t \approx 650$ s) for both tools. We nevertheless note that to slightly increase the convection velocity of the wake, we changed the convection parameter of FAST.Farm (`C_Meander`) to 2.5 from its default value of 1.9. Ignoring the small time offsets, we observe that the curled wake model captures reasonably well the amplitude of the power oscillations, whereas the polar model tends to show higher amplitudes. The minimum value for both FAST.Farm models is close to the steady-state value prior to the oscillatory wake hitting the turbine. For the LES simulation, the minimum power is seen to be greater than the steady-state value. Complex aerodynamic interactions between the vortices of the wake and the waked turbine are likely at play, which are not expected to be captured by FAST.Farm. It is nevertheless expected that as the frequency of the nacelle yaw decreases, the minimum power should reach the steady-state value. Regardless, the new FAST.Farm curl model shows marked improvements over the original FAST.Farm polar model relative to LES.

3.7 | Yaw sweep for two aligned turbines

In this final section, we simulate a case similar to the one investigated in the work of Fleming et al,[33] in which LES simulations were used to study the effect of wake mitigation control strategies—in particular, using yaw control. We simulate two wind turbines separated by 7*D* for a time period of 1 h. We vary the yaw angle of the first turbine while the second turbine remains at a fixed zero-yaw. Both turbines are rigid, the rotational speed is variable, and the land-based NREL 5-MW controller is used. For the simulation, we generated a turbulence box with TurbSim[27] using the Kaimal spectrum, a mean hub-height wind speed of 8 m/s, a turbulence intensity of 11.8%, a power law shear coefficient of 0.1, and

recommended spatial coherence functions. We plot the time-averaged power from the first and second turbine as function of the yaw angle of the first turbine on Figure 16.

We observe that the general trends are captured by the models: the power of the first turbine is reduced for increasing yaw angles due to decreased aerodynamic performances, whereas the opposite occurs for the second turbine, because the wake of the first turbine is deflected away from the second one. Due to the curled wake shape, an asymmetry is expected when the curled wake model is used. In our simulation, we observed an asymmetry both for the curled wake and the polar implementations, where more power is obtained for positive yaw angles compared to negative yaw angles. The trend appears to be consistent with the one observed by Fleming et al,[33] but not as pronounced. The results from Fleming et al. show increased power for positive yaw angles but no gain at negative yaw angles. It is likely that some of the physics at play are not fully captured by the FAST.Farm model and that the shape of the wake deficit (curled or not) is not the main factor responsible for the asymmetry.

We believe that the main driver for the variations observed here is the wake convection, but the curling of the wake is likely to have an effect of second order, which could explain the increased asymmetry observed with the curled wake formulation. The comparison is difficult because the convection is handled differently in the curled wake and polar formulations. We expect the results to vary based on the turbulence box (turbulence intensity, coherence) and the operating conditions, and based on using different values for the tuning constant of FAST.Farm (wake meandering constants, wake deflection parameters). A thorough analysis of the effect of secondary steering and calibration using FAST.Farm will be considered for future work.

4 | CONCLUSION

In this article, we presented a time-varying formulation of the curled wake model that we included into the FAST.Farm framework. We compared results of the original FAST.Farm formulation with a polar-shaped wake with the new formulation, from which we can highlight the following conclusions:

- The study led to several improvements to the baseline formulation of FAST.Farm: (1) A minimum eddy viscosity was introduced to improve the quality of the results when no ambient turbulence is used. (2) Based on the results from the transient yaw event, we obtained a more physical interpretation of the time-filter value and we have now updated the default value of this parameter. (3) The AWAE module now uses a Cartesian implementation, allowing for more versatile wake models in the future. (4) Additional wake outputs were added.
- When comparing the polar and curled wake formulations, small differences were observed in the wake deficits obtained in aligned flows. We believe that these differences result from a lack of enforcement of continuity and the use of an explicit first-order Euler scheme in the curled wake model. Future work should therefore focus on improving the numerical scheme and solving the continuity equation together with the momentum equation, similar to the approach taken in the baseline FAST.Farm wake model. The use of an implicit scheme will also improve the robustness of the algorithm.
- The curled wake formulation includes cross-flow velocities and a realistic wake deficit shape, which are significant improvements to the axisymmetric implementation in conditions with skewed flow. The implementation of the algorithm was verified against LES and a stand-alone version of the curled wake model used in previous publications. The new time-varying implementation of the curled wake model in FAST.Farm shows satisfying agreement with LES, and the results were consistent with previous verification studies of the curled wake model in steady state.
- In spite of the overall agreement, several differences were observed when comparing the curled wake model with the LES results. For the actuator disk results, the lateral convection of the wake center lags in the curled wake model. For the actuator line results, the concentration of vorticity at the top vortex is not as pronounced with the curled wake model. Both observations seem to point to the cross-flow convection and therefore the accuracy of the cross-flow velocities. Improvements can likely be obtained by adapting the vorticity distribution based on the actual circulation distribution at the rotor instead of the integrated thrust coefficient. The present distribution is equivalent to the distribution of a single vortex cylinder (or constant thrust coefficient) concentrated on one line, and improvement might be possible by using a continuous distribution of vorticity radially and azimuthally. A second step would be to convect the vortices within the plane. The vortices currently remain unrealistically fixed along a line, but their location should also curl under their self-induced velocities. Such a modification will be considered in future work.
- The yaw-sweep results indicated that moderate differences were obtained using the curled wake or polar formulation. The curled wake formulation showed increased asymmetry, which is consistent with previously published results using LES. The convection method is likely the first-order factor influencing the power of downstream turbines; the actual symmetry/asymmetry of the deficit is of second order. Both formulations have a different convection algorithm; therefore, the comparison is not straightforward. Future work should continue to investigate the secondary steering obtained with FAST.Farm, focusing on the influence of the various meandering and convection parameters.

ACKNOWLEDGEMENTS

This work was authored by the National Renewable Energy Laboratory, operated by Alliance for Sustainable Energy, LLC, for the US Department of Energy (DOE) under Contract No. DE-AC36-08GO28308. Funding was provided by US Department of Energy Office of Energy Efficiency and Renewable Energy Wind Energy Technologies Office. The views expressed in the article do not necessarily represent the views of the DOE or the US Government. The US Government retains and the publisher, by accepting the article for publication, acknowledges that the US Government retains a nonexclusive, paid-up, irrevocable, worldwide license to publish or reproduce the published form of this work, or allow others to do so, for US Government purposes.

PEER REVIEW

The peer review history for this article is available at https://publons.com/publon/10.1002/we.2785.

DATA AVAILABILITY STATEMENT

The code is available on the OpenFAST repository https://github.com/openfast/openfast. Example test cases are provided in the test repository of OpenFAST.

ORCID

Emmanuel Branlard https://orcid.org/0000-0002-7750-6128
Luis A Martínez-Tossas https://orcid.org/0000-0003-2353-4999

REFERENCES

1. Adaramola MS, Krogstad P-A. Experimental investigation of wake effects on wind turbine performance. *Renew Energy*. 2011;36(8):2078-2086.
2. Fleming P, King J, Dykes K, et al. Initial results from a field campaign of wake steering applied at a commercial wind farm—part 1. *Wind Energy Science*. 2019;4(2):273-285.
3. Glauert H. A general theory of the autogyro. *tech. rep*., H.M. Stationery Office, NACA Reports and Memoranda No. 111; 1926.
4. Coleman RP, Feingold AM, Stempin CW. Evaluation of the induced-velocity field of an idealized helicopter rotor. NACA ARR No L5E10, 1–28; 1945.
5. Branlard E, Gaunaa M. Cylindrical vortex wake model: skewed cylinder, application to yawed or tilted rotors. *Wind Energy*. 2015;19(2):345-358.
6. Branlard E, Meyer Forsting AR. Assessing the blockage effect of wind turbines and wind farms using an analytical vortex model. *Wind Energy*. 2020;23(11):2068-2086. https://doi.org/10.1002/we.2546
7. Bastankhah M, Shapiro C, Shamsoddin S, Gayme D, Meneveau C. A vortex sheet based analytical model of the curled wake behind yawed wind turbines. *J Fluid Mech*. 2022;933:A2.
8. Vollmer L, Steinfeld G, Heinemann D, Kühn M. Estimating the wake deflection downstream of a wind turbine in different atmospheric stabilities: an LES study. *Wind Energy Sci*. 2016;1(2):129-141.
9. Howland MF, Bossuyt J, Martínez-Tossas LA, Meyers J, Meneveau C. Wake structure in actuator disk models of wind turbines in yaw under uniform inflow conditions. *J Renew Sustain Energy*. 2016;8(4):43301.
10. Bastankhah M, Porté-Agel F. Experimental and theoretical study of wind turbine wakes in yawed conditions. *J Fluid Mech*. 2016;806:506-541.
11. Martínez-Tossas LA, Annoni J, Fleming PA, Churchfield MJ. The aerodynamics of the curled wake: a simplified model in view of flow control. *Wind Energy Sci*. 2019;4(1):127-138.
12. Medici D, Alfredsson PH. Measurements on a wind turbine wake: 3d effects and bluff body vortex shedding. *Wind Energy*. 2006;9(3):219-236.
13. Bartl J, Mühle F, Schottler J, Saetran L, Peinke J, Adaramola M, Hölling M. Wind tunnel experiments on wind turbine wakes in yaw: effects of inflow turbulence and shear. *Wind Energy Sci*. 2018;3(1):329-343.
14. Fleming P, Annoni J, Martínez-Tossas LA, Raach S, Gruchalla K, Scholbrock A, Churchfield M, Roadman J. Investigation into the shape of a wake of a yawed full-scale turbine. *J Phys: Confer Ser*. 2018;1037:32010.
15. Schottler J, Bartl J, Mühle F, Sætran L, Peinke J, Hölling M. Wind tunnel experiments on wind turbine wakes in yaw: redefining the wake width. *Wind Energy Sci*. 2018;3(1):257-273.
16. Shapiro CR, Gayme DF, Meneveau C. Modelling yawed wind turbine wakes: a lifting line approach. *J Fluid Mech*. 2018;841:R1.
17. Martínez-Tossas LA, King J, Quon E, Bay CJ, Mudafort R, Hamilton N, Howland MF, Fleming PA. The curled wake model: a three-dimensional and extremely fast steady-state wake solver for wind plant flows. *Wind Energy Sci*. 2021;6(2):555-570.
18. Martínez-Tossas LA, Branlard E. The curled wake model: equivalence of shed vorticity models. *J Phys: Confer Ser*. 2020;1452:12069. https://doi.org/10.1088/1742-6596/1452/1/012069
19. Jonkman J, Shaler K. Fast.farm user's guide and theory manual. *tech. rep*., Golden, CO (US), National Renewable Energy Lab.; 2020.
20. Jonkman JM, Annoni J, Hayman G, Jonkman B, Purkayastha A. Development of fast.farm: a new multi-physics engineering tool for wind-farm design and analysis. *Aiaa Scitech 35th Wind Energy Symposium*: AIAA; 2017.
21. Larsen GC, Madsen Aagaard H, Thomsen K, Larsen TJ. Wake meandering: a pragmatic approach. *Wind Energy*. 2008;11(4):377-395.
22. Branlard E. *Wind Turbine Aerodynamics and Vorticity-Based Methods: Fundamentals and Recent Applications*: Springer International Publishing; 2017.
23. Martnez-Tossas LA, Branlard E, Shaler K, Vijayakumar G, Ananthan S, Sakievich P, Jonkman J. Numerical investigation of wind turbine wakes under high thrust coefficient. *Wind Energy*. 2021;25(4):605-617.
24. Bay CJ, Annoni J, Martnez-Tossas LA, Pao LY, Johnson KE. Flow control leveraging downwind rotors for improved wind power plant operation. In: 2019 american control conference (acc) ACC; 2019:2843-2848.
25. Jonkman J, Butterfield S, Musial W, Scott G. Definition of a 5mw reference wind turbine for offshore system development. *Tech. Rep*. NREL/TP-500-38060, Golden, CO, USA, National Renewable Energy Laboratory; 2009.

26. Doubrawa P, Annoni J, Jonkman J. Optimization-based calibration of fast.farm parameters against large-eddy simulations. AIAA SciTech; 2018.
27. Jonkman BJ, Buhl ML. Turbsim user's guide. *Tech. Rep*. NREL/TP-500-39797, Golden, Colorado, USA, National Renewable Energy Laboratory; 2006.
28. Branlard E, Gaunaa M. Superposition of vortex cylinders for steady and unsteady simulation of rotors of finite tip-speed ratio. *Wind Energy*. 2015; 19(7):1307-1323. https://doi.org/10.1002/we.1899
29. Snel H, Schepers JG. Joint investigation of dynamic inflow effects and implementation of an engineering method. *tech. rep*., Petten, the Netherlands, ECN-C–94-107, Energy Research Centre of the Netherlands; 1995.
30. Cheung L, Brazell MJ, Hsieh A, Ananthan S, Vijayakumar G, deVelder N. Computation and comparison of the stable northeastern us marine boundary layer. In: Aiaa scitech 2021 forum AIAA SciTech; 2021:454.
31. Sprague MA, Ananthan S, Vijayakumar G, Robinson M. Exawind: a multifidelity modeling and simulation environment for wind energy. In: Nawea/windtech 2019 conference, amherst, ma, IOP Publishing; 2019.
32. Abraham A, Martínez-Tossas LA, Hong J. Mechanisms of dynamic near-wake modulation of a utility-scale wind turbine. *J Fluid Mech*. 2021;926:A29.
33. Fleming P, Gebraad PMO, Lee S, van Wingerden J-W, Johnson K, Churchfield M, Michalakes J, Spalart P, Moriarty P. Simulation comparison of wake mitigation control strategies for a two-turbine case. *Wind Energy*. 2015;18(12):2135-2143. https://doi.org/10.1002/we.1810

How to cite this article: Branlard E, Martínez-Tossas LA, Jonkman J. A time-varying formulation of the curled wake model within the FAST.Farm framework. *Wind Energy*. 2023;26(1):44-63. doi:10.1002/we.2785